Surface Science 606 (2012) 902–907

Contents lists available at SciVerse ScienceDirect

Surface Science

journal homepage: www.elsevier.com/locate/susc

pH-dependent structure and energetics of H_2O/MgO(100)

Peter Thissen [a,*], Vera Thissen [b], Stefan Wippermann [c], Yves J. Chabal [a], Guido Grundmeier [b], Wolf Gero Schmidt [c]

[a] Department of Materials Science and Engineering, University of Texas at Dallas, 800 West Campbell Road, Richardson, 75080 TX, USA
[b] Lehrstuhl für Technische und Makromolekulare Chemie, Universität Paderborn, 33098 Paderborn, Germany
[c] Lehrstuhl für Theoretische Physik, Universität Paderborn, 33098 Paderborn, Germany

ARTICLE INFO

Article history:
Received 1 July 2011
Accepted 23 January 2012
Available online 31 January 2012

Keywords:
Magnesium oxide
Water
Adsorption
DFT
pH value
AFM

ABSTRACT

The structure and energetics of water on MgO(100) surfaces are studied by atomic force microscopy (AFM) and density-functional theory (DFT). Computationally, the adsorption of water monomers, small water clusters and water monolayers on MgO(100) surfaces is considered. The calculations predict the non-dissociative adsorption for water monomers. The potential energy surface for single monomers is characterized by very low diffusion barriers. Increasing water coverage leads to the formation of structures containing alternatively dissociated and molecularly adsorbed water molecules. The magnitude of the calculated adsorption energy per water molecule increases from 0.57 eV for the water monomer to 0.79 eV for the water monolayer. The present experimental and theoretical results show furthermore that the stability of MgO(100) surfaces in the presence of water depends on its pH value. The etching of MgO(100) surfaces in aqueous medium is studied with the AFM in situ with pH value changing from basic to acidic. While the atomically flat MgO(100) surface remains stable in basic and neutral pH ranges, it is easily etched when the pH turns below a value of 6. This agrees qualitatively with the present DFT calculations showing that square pits resulting from the etching reduce the MgO(100) surface energy in acidic environments.

1. Introduction

Understanding the chemistry of water/solid interfaces is essential for the understanding of many phenomena in geology, atmospheric chemistry, environmental protection, corrosion, sensors, heterogeneous catalysis and electronics [1,2]. The surface chemistry of most air-formed oxide films on metals changes continuously during ambient storage. The well defined MgO(100) surface has been serving for some time as a model for water interaction with metal oxide surfaces. For example, hydroxide formation and carbonaceous pickup have been quantified at the oxide surface of magnesium [3]. Importantly, hydroxyl formation and carbonaceous adsorption have been found to have opposing effects on the ability of organic molecules to form chemical bonds with the oxide/hydroxide surface. Therefore a detailed characterization of the oxide surface of magnesium stored in ambient conditions is necessary prior to the investigation of the controlled adsorption of organic molecules to this surface. Much work has been carried out on the macroscopic corrosion of magnesium, but less on the changes in the chemistry of its oxide in atmospheric exposure. A clean, unprotected, standard-purity magnesium surface exposed to indoor or outdoor atmospheres will develop a film detectable by eye [4]. In general, atmospheric attack of pure magnesium in damp conditions is believed to result in a superficial MgO layer formed on the pure magnesium metal. In an experiment performed by Nordlien, magnesium has been exposed to ambient atmosphere for 60 min and scratched. After scratching, it developed a film described as a dense mixture of amorphous MgO and crystalline $Mg(OH)_2$ (verified by Transmission Electron Microscopy (TEM) and electron diffraction) [5]. Water adsorption on the MgO(100) surface has also been studied computationally. First-principle calculations were performed, e.g., by Giordano et al., by Odelius as well as by Delle Site et al. [6–8]. From the ab initio calculations, water dissociation on the atomically flat MgO(100) surface was predicted. Semiempirical quantum chemistry calculations, on the other hand, addressed the acidic dissolution of the MgO(100) surface [9]. Recent studies using atomic force microscopy (AFM) report changes in the topography of the MgO(100) surface during dissolution. Rectangular/square pits were reported for the MgO(100) surface in diluted acid (pH 1–2) and in water [10,11]. The pits appear to be of the form of inverted pyramids and are not always symmetric. These pits displayed edges several micrometers in length and would take many minutes to form and reflect the advanced stage of dissolution. Other AFM studies reported the erosion of steps and edges due to the exposure of MgO to high humidity. These studies, however, did not report the formation of etched pits [12–14].

* Corresponding author.
E-mail address: peter.thissen@utdallas.edu (P. Thissen).

0039-6028/$ – see front matter © 2012 Elsevier B.V. All rights reserved.
doi:10.1016/j.susc.2012.01.018

Here, we explore the structure and energetics of both molecularly and dissociatively adsorbed water for various coverages by density-functional theory (DFT) calculations. The potential energy surface (PES) for surface adsorbed water monomers is determined in order to address the question of water mobility on the MgO(100) surface. In addition, the stability of MgO(100) in aqueous media as a function of the pH value is investigated by in situ AFM as well as by ab initio total-energy calculations.

2. Experimental

All chemical reagents were of analysis grade and were used without any further purification. The MgO(100) crystals were purchased at MaTecK (MaTecK GmbH, Juelich, Germany) with an accuracy of +/−0.5°, a size of 20 mm×20 mm (+/−0.1 mm), a thickness of 0.5 mm (+/−0.05 mm) and an edge orientation along <010>/<001>. One side was polished. The surfaces were prepared as follows: before annealing, the crystals were immersed into 85% phosphoric acid (Aldrich) for 1 min, rinsed with deionized water (resistivity = 18.2 k Ω) and dried in a stream of nitrogen. The crystals were then annealed in a high temperature oven (Carbolight, RHF15-3) for 360 min at 1000 °C [15]. For the solutions with the adjusted pH value of 11 and 6, three base solutions were prepared: $NaClO_4$ (99.99%, Aldrich) as base electrolyte, NaOH (0.2 mol/l, VWR) and $HClO_4$ (10 mM, Fluka). They were all diluted to 1 mM to ensure, that every pH value is of the same ionic strength and then mixed to pH 11 and pH 6. Additionally, the electrolyte was purged with argon for all measurements to avoid any effects due to CO_2 contamination. Perchlorate was chosen as the anion because it does not promote the dissolution process by any surface complexation.

The AFM images were obtained with an Agilent 5100 (Agilent Technologies) in fluid and all images are of the size 2 μm×2 μm. The sample was mounted in a purchased open fluid cell with tube connections, which were connected with a MDSP3f syringe pump (MMT Micro Mechatronic Technologies GmbH, Siegen) for a continuous fluid exchange, while the flow was adjusted to 500 μl/min. The cantilevers were of the type NSC19/no Al with the typical resonance frequency of 80 kHz and a typical spring constant of 0.6 N/m (Mikro Masch/Anfatec, Oelsnitz, Germany).

3. Theory

The calculations were performed using DFT within the generalized gradient approximation (GGA) as implemented in the Vienna ab initio simulation package (VASP) [16,17]. The electron–ion interaction is described by the projector-augmented wave scheme (PAW) [18]. The electronic wave functions are expanded into plane waves up to a kinetic energy of 440 eV. This energy cutoff was found to result in converged lattice parameters and bulk modulus for both bulk MgO and water (ice_{Ih}). The surface is modeled by periodically repeated slabs. The supercells used here consist of 6 atomic layers within a 2×3 surface periodicity plus adsorbed water and a vacuum region equivalent to 6 atomic layers. The 5 uppermost layers as well as the adsorbate degrees of freedom are allowed to relax until the forces on the atoms are below 20 meV/Å. The Brillouin zone integration is performed using 3×3×1 Monkhorst–Pack meshes. We use the PW91 functional to describe the electron exchange and correlation energy within the GGA [19]. It describes the hydrogen bonds in solid water (ice_{Ih}) in good agreement with experimental results [20,21].

4. Results

Bulk MgO has rock-salt symmetry with a lattice constant of 0.421 nm. In good agreement with previous studies [6–8], we find only very small structural relaxations of the clean MgO(100) surface. We start the adsorption study by determining the PES for a single water monomer on the clean MgO(100) surface. Apart from the lateral position of the oxygen atom of water, all structural degrees of freedom of both substrate and adsorbate were fully relaxed in these calculations. The calculated data are shown in Fig. 1 (lhs). In order to account for the fact that energy barriers hinder the free rotation of surface adsorbed water molecules, the minimum energy geometry for every PES sampling point was obtained by probing different molecular starting orientations. As can be seen in Fig. 1 (rhs), the energetic favored diffusion pathway passes the hollow position as transition state with an energy barrier of only 0.03 eV.

Starting from the lowest energy adsorption configuration of a single water monomer on the (3×2) surface unit cell, the water coverage was systematically increased to six water molecules, corresponding to one monolayer of water. The corresponding lowest energy structures obtained from various starting geometries for the respective water coverage on the MgO(100)-(3×2) surface are shown in Fig. 2. Here and in the following the notation M*n* refers to structures with *n* water molecules per (3×2) unit cell. Fig. 3 depicts the adsorption energy E_{ads} as a function of the number of water molecules adsorbed on the MgO(100) surface. It is calculated from the energies of the water adsorbed surface containing n molecules, (E_n) the gas-phase water molecule (E_{H2O}) and the clean slab (E_0) as:

$$E_{ads} = \frac{E_n - E_0 - n * E_{H_2O}}{n}.$$

We find the magnitude of the adsorption energy to increase nearly monotonously with increasing coverage for the different adsorption geometries, due to the water–water interaction. However, the sign of the adsorption energy alone does not allow to conclude on the stability of a specific surface structure. Rather, one has to take into account the chemical potentials $\mu(A_i)$ of the surface constituents A_i in order to compare interfaces with different stoichiometries energetically (see, e.g. Refs. [22,23]). The ground state of the surface is determined by the minimum of the thermodynamic grandcanonical potential

$$\Omega = F - \sum_i \mu(A_i) * n_{A_i} + q * (E_F + E_{VBM})$$

where $F = E - TS$ is the surface free energy which we approximate by the total surface energy E at zero temperature assuming similar entropy contributions S for different adsorption configurations. In fact, the differences in vibrational free energy and electronic entropy are typically several orders of magnitude smaller than the adsorption energies calculated here, see, e.g. Ref. [24]. The last term on the right hand side accounts for the energy changes due to a possible surface charge q in dependence on the electron chemical potential given here by the Fermi level E_F measured relative to the MgO valence-band maximum, E_{VBM}.

If one assumes a neutral and flat, i.e., stoichiometric, MgO(100) surface in the presence of pure water, the grandcanonical potential will only depend on the number and chemical potential $\mu(H_2O)$ of the water molecules.

Fig. 4 shows the resulting phase diagram. Here two important values are indicated. Extreme water-rich conditions are marked by a vertical line denoted $\mu_{solid}(H_2O)$. This value corresponds to a MgO(100) surface in equilibrium with bulk water approximated here by calculations for ice_{Ih}. The corresponding calculations for bulk water (ice_{Ih}) reproduce the data obtained in an earlier work of one of the present authors; given as Ref. [21]. Lower values of $\mu(H_2O)$ indicate an increasingly dry environment. The zero-temperature calculation for gas-phase water molecules is indicated by another vertical line $\mu_{gas}(H_2O)$. The phase diagram shows that out of the six energetically favorable structures shown in Fig. 2 only three structures (besides the clean surface) are in fact thermodynamically stable as well: these are the monomer for low water supply (M1), the monolayer for water-rich conditions (M6) and a 2×2+1

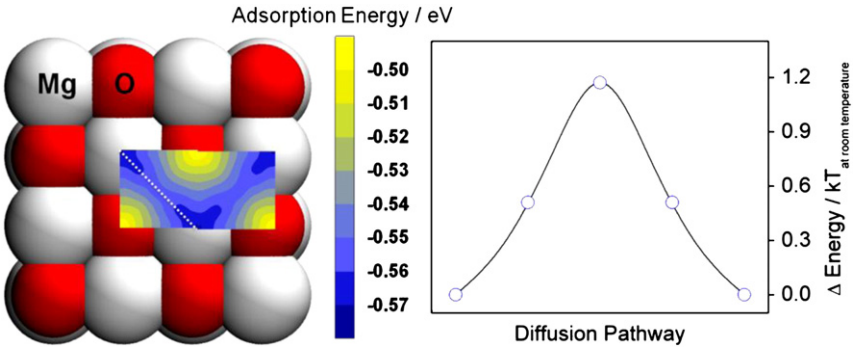

Fig. 1. (lhs) Potential energy surface (PES) for a water monomer on the MgO(100) surface. (rhs) Energy profile along the white dashed line (favorable diffusion pathway) in the PES.

cluster for intermediate conditions (M5). Obviously, for very water-rich conditions structures with coverage exceeding one monolayer (not considered here) will form.

Next we consider the case where the surface is in equilibrium with bulk water with a specific pH value. Fig. 5 shows the AFM topographies all taken in one in situ measurement. The experiment was started at pH 11 and as soon as the image had stabilized the solution was changed from pH 11 to pH 6. The electrolyte output was controlled by measuring the pH value. One can see clearly that the MgO(100) surface keeps the single crystalline topography in basic pH ranges. This stability is lost as soon as the pH value turns acidic. As can be seen in Fig. 5 the etching process does not start from steps, kinks or other specific defects. In accordance with the square pit etching mechanism already earlier observed experimentally, see, e.g., Ref. [11], we find a homogeneous distribution of etch defects that grow deeper with time. The proposed mechanisms (see also Ref. [9]) involve the step-wise dissolution from the initial planar MgO(100) surface.

In order to model this process atomically, we consider a scenario of 4 hydrogen atoms and one water molecule adsorbed on the MgO(100)-(3×2) unit cell. We do not calculate charges specifically associated with each H atom because it is beyond the limits of this density functional theory studies to correlate a specific number of electrons to specific atomic positions in the unit cell. In accordance with experimental findings this unit cell is not charged in the basic pH range (pzc for MgO = 12.4 [34]). It is charged to investigate the stability of the unit cell as a function of the pH value. The chemical potential of the protons increases when the pH value is changing from basic to acidic. It is considered that Mg atoms are substituted by two protons. The concept behind this mechanism is based on the square pits observed by AFM measurements. Water adsorbed on the surface stabilizes the charged structures. The number of water molecules included in our model structures had to be kept to a minimum for computational reasons. Even though the model is not realistic at very basic pH values, it is still very useful to start the modeling from high pH values to better see the trend as the pH value is lowered into acidic ranges. The model is realistic for the neutral and acidic pH ranges. Here and in the following the notation Mxy^{z+} refers to structures that have x Mg atoms less and y adsorbed hydrogen atoms more per (3×2) unit cell; z denotes to the charge state of the unit cell. Employing the MgO(100)-(3×2) surface unit cell we investigate by DFT an extensive set of more than 30 configurations with surface structures including vacancies and adsorbates, both electrically charged and neutral. The energetically most relevant structures used to model the square pit etching mechanism can be seen in Fig. 6. For the calculations with charged supercells we assume a neutralizing background charge.

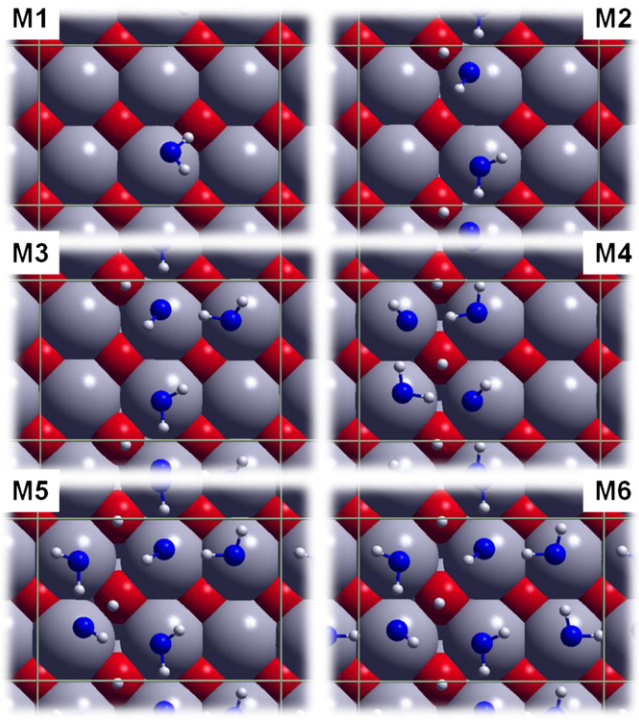

Fig. 2. Energetically favorable adsorption structures of water on MgO(100). The water coverage is increasing from monomer (M1) to monolayer (M6). Mg is represented by silver spheres, O in MgO is represented by red spheres, O in water is represented by blue spheres and H is represented by white spheres. The unit cell used in the calculations is indicated.

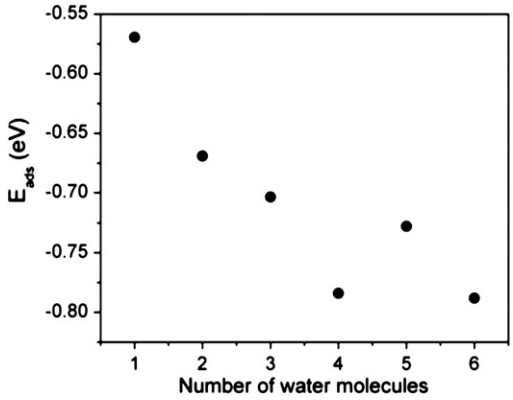

Fig. 3. Calculated adsorption energy (per molecule) as a function of the number of water molecules within the MgO(100) (2×3) surface unit cell.

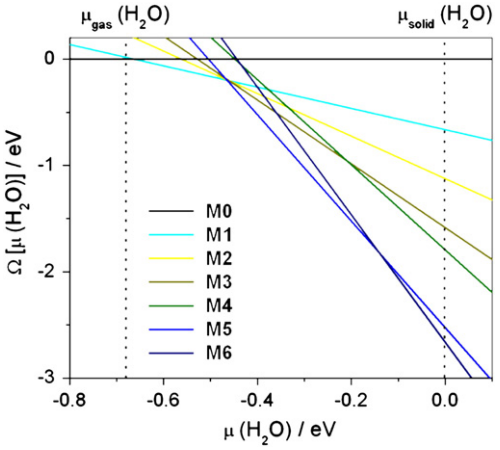

Fig. 4. Calculated phase diagram of the clean (M_0) and water-adsorbed MgO(100) surface as a function of the chemical potential of water with respect to its bulk value, approximated here by calculations for ice_{Ih}.

In order to assess the stability of the various model structures we again calculate the thermodynamic grandcanonical potential. However, now additional degrees of freedom enter: not only the number of water molecules, but also the numbers of surface Mg and O atoms as well as H and electrons will not be the same anymore for different structures. While the chemical potentials of the surface constituents Mg and O are not independent from each (their sum is here assumed to equal the MgO bulk chemical potential, for a detailed discussion see, e.g., Refs. [22,23]) and the oxygen and hydrogen chemical potential are related to the water chemical potential, there still remain three degrees of freedom. They can be chosen to the water, proton, and electron chemical potentials. In the following we assume the water chemical potential to equal $\mu_{solid}(H_2O)$, i.e., assume the system to be in equilibrium with bulk water. The electron chemical potential is assumed to be fixed at the valence-band maximum (VBM) of the ideal crystal. It is determined here from the energy difference between a slightly charged (0.001 *e*) and a neutral MgO cell (see, e.g., Ref. [25]). For the determination of the chemical potential of the protons, we follow the approach suggested, e.g., by Himmel et al. [26] and use:

$$\mu\left(H^+\right) = \mu_0 - \mathrm{pH} * 0.05918\, eV$$

where μ_0 contains the proton solvation enthalpy in water. The hydrogen chemical potential is shifted with respect to the H^+ chemical potential by the electron binding energy in hydrogen with respect to the electron chemical potential. The former is calculated here again from the difference in energy between the slightly charged and the neutral gas-phase hydrogen atom. The present choice of independent and pinned chemical potentials allows for comparing the stability of the proposed model structures in dependence on the pH value only. The resulting one-dimensional phase diagram is shown in Fig. 7. In qualitative agreement with our experimental findings initial defect structures (represented here by the $M14^{4+}$ model) become energetically favorable over the flat MgO(100) surface for pH values below ~7. Larger defects such as $M26^{6+}$ are stabilized at even lower pH values (around 6). The calculations also predict a tendency for positive surface charging with lower pH values, at least for electron chemical potentials close to the MgO VBM. A word of caution is certainly in order with respect to the calculated phase diagram. Some of the assumptions made for its construction are certainly approximations. The choice of the Mg chemical potential, for example, is ambiguous, since the considered system is not in thermodynamic equilibrium. Also, the number of structures and charge states that can be considered is certainly limited and we cannot be sure to include all relevant interface compositions.

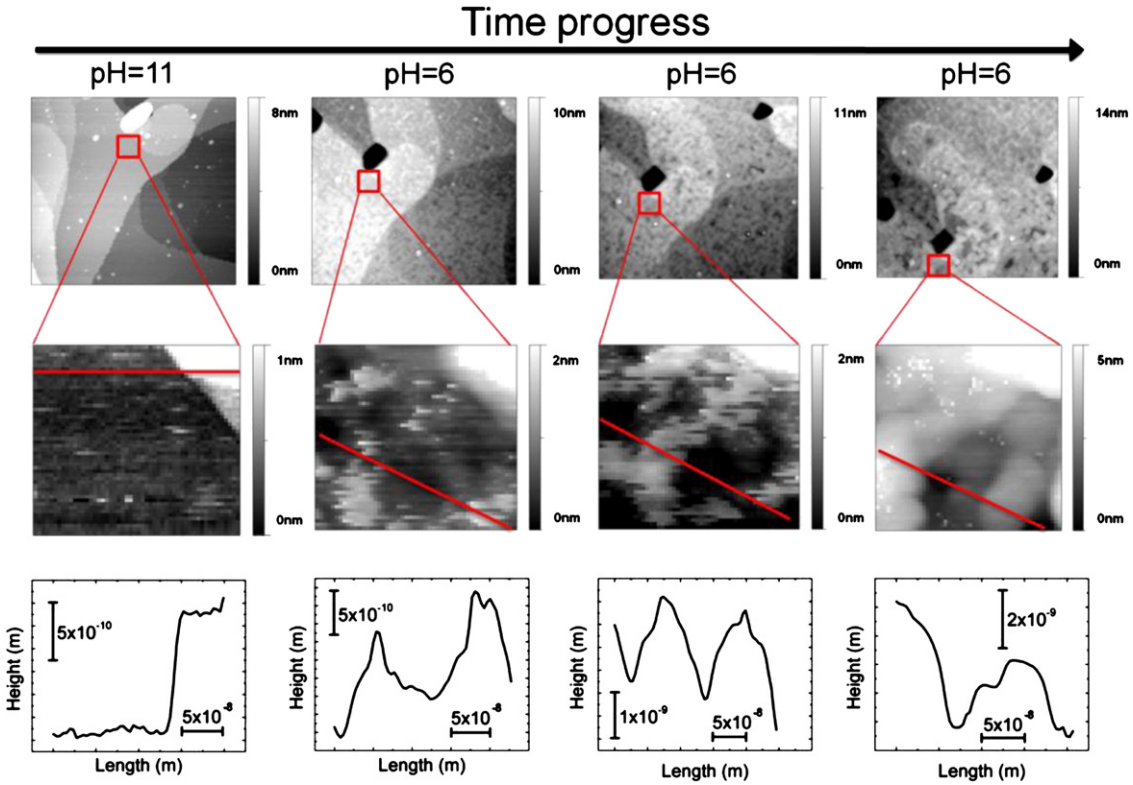

Fig. 5. In situ AFM topographies and cross-sections of the MgO(100) surface in water at different pH values. The solid/liquid interface indicates dissolution when the pH value turns acidic. Upper line images represent scans of $2 \times 2\ \mu m^2$, bottom line images represent zooms of $200 \times 200\ nm^2$. Cross-sections are marked by solid red lines in the zoom ins.

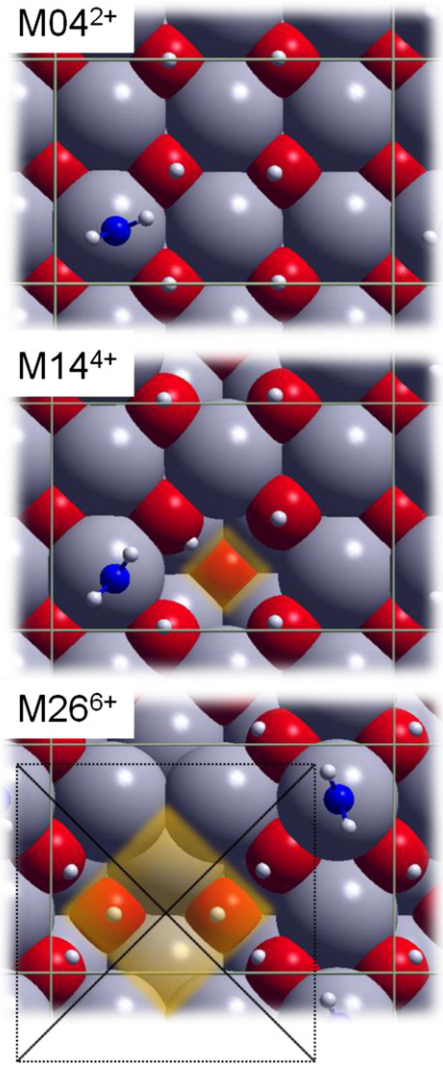

Fig. 6. Top views of some energetically relevant structures used to model the square pit etching mechanism of MgO(100). Mg is represented by silver spheres, O in MgO is represented by red spheres, O in water is represented by blue spheres and H is represented by white spheres. Transparent red regions indicate the etched pits. In M26^{6+} an inverted pyramidal structure is painted as guide to the eyes. Its sidewalls have MgO(111) orientation.

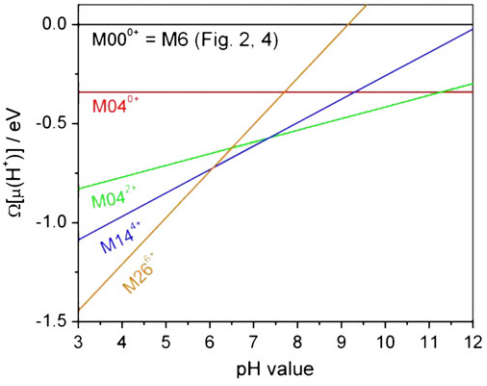

Fig. 7. Calculated phase diagram of clean and etched MgO(100) surface structures as a function of the pH value. Out of the calculated structures only the energetically favorable models are shown. Positively charged defect structures are favorable for pH values lower than about 7.

Additionally, we neglect temperature effects in the chemical potentials. Still, the theoretical finding that acid environments favor structures set up according to the square pit etching mechanism lends credibility to these models and provides a plausible microscopic interpretation of our experimental results.

5. Discussion

For low values of the water chemical potential, single adsorbed water monomers are thermodynamically stable. The water molecule is sitting close to the top position on the Mg atom and binds via the OH group hydrogen to the next surface oxygen. For increasingly water-rich environment the M5 (cf. Fig. 2) becomes favorable. The $2\times2+1$ cluster contains two dissociated water molecules that are stabilized in a subtle network of hydrogen bonds. For even higher values of the water chemical potential the calculations predict the formation of a water monolayer structure (M6 in Fig. 2), where two out of six water molecules dissociate. Thereby they transfer their protons to neighboring surface oxygen atoms. The dissociated molecules are stabilized by molecularly adsorbed water monomers in their vicinity that adsorb nearly parallel to the MgO(100) surface. They shift horizontally (with respect to the position of isolated monomers) and approach closely the dissociated water molecules. The short oxygen–oxygen distance between these two molecules and the orientation of their OH group indicate the existence of a hydrogen bond. Although two water molecules form what can be regarded as a water dimer, the presence of the substrate noticeably modifies its properties. This is reflected by a shorter oxygen–oxygen distance and a dimerization-induced proton transfer towards the surface oxygen. This situation is similar to that reported already for the water adsorption on the surface of TiO_2(110). In that case, an enhanced mobility of the hydrogen atom along water-surface hydrogen bond leads to a coexistence of molecular and dissociated water, stabilized by a mutual hydrogen bond [27]. The coexistence of dissociative and molecularly adsorbed water molecules has recently been found also on other oxide surfaces such as α-Al_2O_3(0001) and Fe_3O_4(0001) [28,29]. Upon adsorption, the OH bonds of water molecules become inequivalent. This is reflected by changes of their length with respect to a free water molecule. The OH bonds incorporated into hydrogen bonding are ~12% longer. The hydrogens transferred to the MgO surface upon water dissociation to form OH bonds. The formation of these bonds was earlier assumed to require surface defects [30]. Our results show that the surface hydroxyl groups may also exist on an atomically flat MgO(100) surface. This indicates the possibility that the sharp bands observed in FTIR experiments [31] arise from dissociated water vibrating on the intact surface. Furthermore, the spontaneous dissociation suggests a mechanism, without reference to defects, for the dissolution of the MgO(100) surface.

The most stable surface of crystalline MgO in vacuum is the (100) plane. While atoms in the bulk are octahedrally coordinated, atoms at the (100) surface are typically fivefold coordinated. Low coordination sites at corners and steps or defect sites are generally accepted as initiation sites for reactions including dissolution [32]. Interestingly, this study – in accordance with earlier semiempirical work [9] – proposes that defects are not necessary to initiate dissolution. While a thorough theoretical treatment of the dissolution process requires methodologies beyond the present total-energy calculations (see, e.g. Ref. [33]) already the present thermodynamic results clearly show that etching resulting in square pits is energetically favorable in acid solution. In fact, this is to be expected: as a basic oxide, MgO naturally has a high affinity for protons. This is reflected in surface charge measurements of MgO that requires a pH of 12.4 in order to obtain surface neutrality [34]. For lower pH values, the dominant charged species are protons. Therefore, it appears plausible that Mg–O pairs tend to migrate out of the surface plane. The present

calculations show that the MgO(100) surface may induce water dimerization and subsequent dissociation within a monolayer of water. Sidewalls of the inverted pyramids growing as square pits have MgO(111) orientation (see Fig. 6) and the fully hydroxylated MgO(111) represents the thermodynamic ground state of MgO in the presence of water. Mg exposed to water at room temperature forms an oxide film and is converted to $Mg(OH)_2$ [3], which is stable in basic ranges of the pH value but not in the acidic ranges. Thus, our findings are consistent with the Pourbaix-diagram from Ref. [35].

6. Conclusions

In the energetically favored alternating dissociated and molecular states identified in this study the water molecules dissociate by transferring a proton to hydroxylate the surface. An important factor in the stabilization of these structures is the formation of strong hydrogen bonds from non-dissociated water molecules to the OH in the adsorbed water layer. This suggests that the maximum number of dissociated near surface water molecules is likely to be 50%. The stability of the interface is determined by a subtle balance between the maintenance of the hydrogen bond network within the water layer and the formation of hydrogen bonds to the oxide ions in the surface layer.

In the case of MgO(100) in diluted acid, we have shown that dissolution can occur from the atomically flat MgO(100) surface without surface defects. The adsorption of protons and water is necessary to promote this process. From the thermodynamical point of view, the square pit etching mechanism is favorable. The probability of defect and charged arrangements increases significantly as the pH value decreases. This is in qualitative agreement with our experimental observations from the AFM.

Acknowledgments

The authors gratefully acknowledge the DFG for their financial support. We thank the Paderborn Center for Parallel Computing (PC^2), the High Performance Computing Center Stuttgart (HLRS) as well as the Texas Advanced Computing Center (TACC) for computational resources.

References

[1] H.J. Freund, H. Kuhlenbeck, V. Staemmler, Rep. Prog. Phys. 59 (3) (1996) 283.
[2] P.A. Thiel, T.E. Madey, Surf. Sci. Rep. 7 (6–8) (1987) 211.
[3] C. Fotea, J. Callaway, M.R. Alexander, Surf. Interface Anal. 38 (10) (2006) 1363.
[4] J. Kim, K.C. Wong, P.C. Wong, S.A. Kulinich, J.B. Metson, K.A.R. Mitchell, Appl. Surf. Sci. 253 (9) (2007) 4197.
[5] J.H. Nordlien, S. Ono, N. Masuko, K. Nisancioglu, J. Electrochem. Soc. 142 (10) (1995) 3320.
[6] L. Giordano, J. Goniakowski, J. Suzanne, Phys. Rev. Lett. 81 (6) (1998) 1271.
[7] M. Odelius, Phys. Rev. Lett. 82 (19) (1999) 3919.
[8] L. Delle Site, A. Alavi, R.M. Lynden-Bell, J. Chem. Phys. 113 (8) (2000) 3344.
[9] D.J. Simpson, T. Bredow, R.S.C. Smart, A.R. Gerson, Surf. Sci. 516 (1–2) (2002) 134.
[10] J.A. Mejias, A.J. Berry, K. Refson, D.G. Fraser, Chem. Phys. Lett. 314 (5–6) (1999) 558.
[11] M.F. Suarez, R.G. Compton, J. Phys. Chem. B 102 (37) (1998) 7156.
[12] D. Abriou, J. Jupille, Surf. Sci. 430 (1–3) (1999) L527.
[13] S.A. Holt, C.F. Jones, G.S. Watson, A. Crossley, C. Johnston, C.J. Sofield, S. Myhra, Thin Solid Films 292 (1–2) (1997) 96.
[14] P. Liu, T. Kendelewicz, G.E. Brown, G.A. Parks, P. Pianetta, Surf. Sci. 416 (1–2) (1998) 326.
[15] S. Benedetti, P. Torelli, P. Luches, E. Gualtieri, A. Rota, S. Valeri, Surf. Sci. 601 (13) (2007) 2636.
[16] G. Kresse, J. Furthmuller, Comput. Mater. Sci. 6 (1) (1996) 15.
[17] G. Kresse, J. Furthmuller, Phys. Rev. B 54 (16) (1996) 11169.
[18] G. Kresse, D. Joubert, Phys. Rev. B 59 (3) (1999) 1758.
[19] J.P. Perdew, J.A. Chevary, S.H. Vosko, K.A. Jackson, M.R. Pederson, D.J. Singh, C. Fiolhais, Phys. Rev. B 46 (11) (1992) 6671.
[20] D.R. Hamann, Phys. Rev. B 55 (16) (1997) 10157.
[21] C. Thierfelder, A. Hermann, P. Schwerdtfeger, W.G. Schmidt, Phys. Rev. B 74 (4) (2006) 045422.
[22] G.X. Qian, R.M. Martin, D.J. Chadi, Phys. Rev. B 38 (11) (1988) 7649.
[23] S. Sanna, W.G. Schmidt, Phys. Rev. B 81 (21) (2010) 214116.
[24] S. Wippermann, W.G. Schmidt, Phys. Rev. Lett. 105 (12) (2010).
[25] L.S. dos Santos, W.G. Schmidt, E. Rauls, Phys. Rev. B 84 (11) (2011) 115201.
[26] D. Himmel, S.K. Goll, I. Leito, I. Krossing, Angew. Chem. Int. Ed. 49 (38) (2010) 6885.
[27] P.J.D. Lindan, N.M. Harrison, M.J. Gillan, Phys. Rev. Lett. 80 (4) (1998) 762.
[28] P. Thissen, G. Grundmeier, S. Wippermann, W.G. Schmidt, Phys. Rev. B 80 (24) (2009) 245403.
[29] N. Mulakaluri, R. Pentcheva, M. Wieland, W. Moritz, M. Scheffler, Phys. Rev. Lett. 103 (17) (2009).
[30] W. Langel, M. Parrinello, Phys. Rev. Lett. 73 (3) (1994) 504.
[31] J. Heidberg, B. Redlich, D. Wetter, Ber. Bunsen Ges. Phys. Chem. Chem. Phys. 99 (11) (1995) 1333.
[32] M. Valtiner, S. Borodin, G. Grundmeier, Langmuir 24 (10) (2008) 5350.
[33] M.A. Gosalvez, Y. Xing, K. Sato, R.M. Nieminen, J. Micromech. Microeng. 18 (5) (2008) 055029.
[34] M. Kosmulski, Chemical Properties of Material Surfaces, Marcel Dekker AG, New York, 2001 Book.
[35] M. Pourbaix, Atlas of Electrochemical Equilibria in Aqueous Solutions, National Association of Corrosion Engineers, 1974.